Lipid detection in atherosclerotic human coronaries by spectroscopic intravascular photoacoustic imaging

Krista Jansen,[1,2] Min Wu,[1] Antonius F. W. van der Steen,[1,2,3] and Gijs van Soest[1,*]

[1]*Department of Biomedical Engineering, Erasmus Medical Center, PO Box 2040, 3000 CA Rotterdam, The Netherlands*

[2]*Interuniversity Cardiology Institute of The Netherlands – Netherlands Heart Institute, PO Box 19258, 3501 DG Utrecht, The Netherlands*

[3] *Department of Imaging Science and Technology, Delft University of Technology, Lorentzweg 1, 2628 CJ Delft, The Netherlands*

[*] *g.vansoest@erasmusmc.nl*

Abstract: The presence of lipids in atherosclerotic coronary lesions is an important determinant of their potential to trigger acute coronary events. Spectroscopic intravascular photoacoustic imaging (sIVPA) has the potential to automatically detect lipids in atherosclerotic lesions. For real-time in vivo imaging, limiting the number of excitation wavelengths is crucial. We explored methods for plaque lipid detection using sIVPA, with the aim to minimize the number of laser pulses per image line. A combined intravascular ultrasound (IVUS) and photoacoustic imaging system was used to image a vessel phantom and human coronary arteries ex vivo. We acquired co-registered cross-sectional images at several wavelengths near 1200 nm, a lipid-specific absorption band. Correlating the photoacoustic spectra at 6 or 3 wavelengths from 1185 to 1235 nm with the absorption spectrum of cholesterol and peri-adventitial tissue, we could detect and differentiate the lipids in the atherosclerotic plaque and peri-adventitial lipids, respectively. With two wavelengths, both plaque and peri-adventitial lipids were detected but could not be distinguished.

OCIS codes: (170.7170) Photoacoustic imaging; (110.4234) Multispectral and hyperspectral imaging; (170.6935) Tissue characterization; (170.2150) Endoscopic imaging; (170.7170) Ultrasound; (170.3880) Medical and biological imaging.

References and links

1. Global atlas on cardiovascular disease prevention and control.," (World Health Organization, Geneva, 2011).
2. E. Falk, P. K. Shah, and V. Fuster, "Coronary Plaque Disruption," Circulation **92**(3), 657–671 (1995).
3. J. A. Schaar, J. E. Muller, E. Falk, R. Virmani, V. Fuster, P. W. Serruys, A. Colombo, C. Stefanadis, S. Ward Casscells, P. R. Moreno, A. Maseri, and A. F. W. van der Steen, "Terminology for high-risk and vulnerable coronary artery plaques. Report of a meeting on the vulnerable plaque," Eur. Heart J. **25**(12), 1077–1082 (2004).
4. R. Virmani, F. D. Kolodgie, A. P. Burke, A. Farb, and S. M. Schwartz, "Lessons from sudden coronary death: A comprehensive morphological classification scheme for atherosclerotic lesions," Arterioscler. Thromb. Vasc. Biol. **20**(5), 1262–1275 (2000).
5. P. D. Richardson, M. J. Davies, and G. V. Born, "Influence of plaque configuration and stress distribution on fissuring of coronary atherosclerotic plaques," Lancet **334**(8669), 941–944 (1989).
6. C. V. Felton, D. Crook, M. J. Davies, and M. F. Oliver, "Relation of Plaque Lipid Composition and Morphology to the Stability of Human Aortic Plaques," Arterioscler. Thromb. Vasc. Biol. **17**(7), 1337–1345 (1997).
7. C. L. Korte, A. F. W. Steen, E. I. Cépedes, G. Pasterkamp, S. G. Carlier, F. Mastik, A. H. Schoneveld, P. W. Serruys, and N. Bom, "Characterization of plaque components and vulnerability with intravascular ultrasound elastography," Phys. Med. Biol. **45**(6), 1465–1475 (2000).
8. A. Nair, B. D. Kuban, E. M. Tuzcu, P. Schoenhagen, S. E. Nissen, and D. G. Vince, "Coronary plaque classification with intravascular ultrasound radiofrequency data analysis," Circulation **106**(17), 2200–2206 (2002).

#192725 - $15.00 USD Received 21 Jun 2013; revised 29 Jul 2013; accepted 25 Aug 2013; published 5 Sep 2013

9. T. Thim, M. K. Hagensen, D. Wallace-Bradley, J. F. Granada, G. L. Kaluza, L. Drouet, W. P. Paaske, H. E. Bøtker, and E. Falk, "Unreliable assessment of necrotic core by Virtual Histology intravascular ultrasound in porcine coronary artery disease," Circ Cardiovasc Imaging **3**(4), 384–391 (2010).
10. J. F. Granada, D. Wallace-Bradley, H. K. Win, C. L. Alviar, A. Builes, E. I. Lev, R. Barrios, D. G. Schulz, A. E. Raizner, and G. L. Kaluza, "In vivo plaque characterization using intravascular ultrasound-virtual histology in a porcine model of complex coronary lesions," Arterioscler. Thromb. Vasc. Biol. **27**(2), 387–393 (2006).
11. E. S. Shin, H. M. Garcia-Garcia, J. M. Ligthart, K. Witberg, C. Schultz, A. F. van der Steen, and P. W. Serruys, "In vivo findings of tissue characteristics using iMap™ IVUS and Virtual Histology™ IVUS," EuroIntervention **6**(8), 1017–1019 (2011).
12. G. van Soest, T. Goderie, E. Regar, S. Koljenović, G. L. J. H. van Leenders, N. Gonzalo, S. van Noorden, T. Okamura, B. E. Bouma, G. J. Tearney, J. W. Oosterhuis, P. W. Serruys, and A. F. W. van der Steen, "Atherosclerotic tissue characterization in vivo by optical coherence tomography attenuation imaging," J. Biomed. Opt. **15**(1), 011105 (2010).
13. C. M. Gardner, J. Lisauskas, E. L. Hull, H. Tan, S. Sum, T. Meese, C. Jiang, S. Madden, J. Caplan, and J. E. Muller, "A catheter-based near-infrared scanning spectroscopy system for imaging lipid-rich plaques in human coronary arteries in vivo," Proc. SPIE **67650**, 67650G, 67650G-8 (2007).
14. S. Garg, P. W. Serruys, M. van der Ent, C. Schultz, F. Mastik, G. van Soest, A. F. van der Steen, M. A. Wilder, J. E. Muller, and E. Regar, "First use in patients of a combined near infra-red spectroscopy and intra-vascular ultrasound catheter to identify composition and structure of coronary plaque," EuroIntervention **5**(6), 755–756 (2010).
15. D. Razansky, C. Vinegoni, and V. Ntziachristos, "Multispectral photoacoustic imaging of fluorochromes in small animals," Opt. Lett. **32**(19), 2891–2893 (2007).
16. J. Laufer, D. Delpy, C. Elwell, and P. Beard, "Quantitative spatially resolved measurement of tissue chromophore concentrations using photoacoustic spectroscopy: application to the measurement of blood oxygenation and haemoglobin concentration," Phys. Med. Biol. **52**(1), 141–168 (2007).
17. K. Jansen, A. F. W. van der Steen, H. M. M. van Beusekom, J. W. Oosterhuis, and G. van Soest, "Intravascular photoacoustic imaging of human coronary atherosclerosis," Opt. Lett. **36**(5), 597–599 (2011).
18. B. Wang, A. Karpiouk, D. Yeager, J. Amirian, S. Litovsky, R. Smalling, and S. Emelianov, "In vivo intravascular ultrasound-guided photoacoustic imaging of lipid in plaques using an animal model of atherosclerosis," Ultrasound Med. Biol. **38**(12), 2098–2103 (2012).
19. T. J. Allen, A. Hall, A. P. Dhillon, J. S. Owen, and P. C. Beard, "Spectroscopic photoacoustic imaging of lipid-rich plaques in the human aorta in the 740 to 1400 nm wavelength range," J. Biomed. Opt. **17**(6), 061209–061210 (2012).
20. H. W. Wang, N. Chai, P. Wang, S. Hu, W. Dou, D. Umulis, L. V. Wang, M. Sturek, R. Lucht, and J. X. Cheng, "Label-free bond-selective imaging by listening to vibrationally excited molecules," Phys. Rev. Lett. **106**(23), 238106 (2011).
21. K. Jansen, G. Springeling, C. Lancee, R. Beurskens, F. Mastik, A. F. W. van der Steen, and G. van Soest, "An intravascular photoacoustic imaging catheter," in International Ultrasonics Symposium (IUS), 2010 IEEE, 2010), 378–381.
22. Q. Zhou, X. Xu, E. J. Gottlieb, L. Sun, J. M. Cannata, H. Ameri, M. S. Humayun, P. Han, and K. K. Shung, "PMN-PT single crystal, high-frequency ultrasonic needle transducers for pulsed-wave Doppler application," IEEE Trans. Ultrason. Ferroelectr. Freq. Control **54**(3), 668–675 (2007).
23. C. L. Tsai, J. C. Chen, and W. J. Wang, "Near-infrared absorption property of biological soft tissue constituents," J. Med. Biol. Eng. **21**, 7–14 (2001).
24. B. Lundberg, "Chemical composition and physical state of lipid deposits in atherosclerosis," Atherosclerosis **56**(1), 93–110 (1985).
25. C. Stegemann, I. Drozdov, J. Shalhoub, J. Humphries, C. Ladroue, A. Didangelos, M. Baumert, M. Allen, A. H. Davies, C. Monaco, A. Smith, Q. Xu, and M. Mayr, "Comparative lipidomics profiling of human atherosclerotic plaques," Circ Cardiovasc Genet **4**(3), 232–242 (2011).
26. P. Wang, P. Wang, H.-W. Wang, and J.-X. Cheng, "Mapping lipid and collagen by multispectral photoacoustic imaging of chemical bond vibration," J. Biomed. Opt. **17**(9), 096010 (2012).
27. J. Glatz, N. C. Deliolanis, A. Buehler, D. Razansky, and V. Ntziachristos, "Blind source unmixing in multi-spectral optoacoustic tomography," Opt. Express **19**(4), 3175–3184 (2011).

1. Introduction

Coronary atherosclerosis is the largest cause of death in Western countries [1]. Most myocardial infarctions are triggered by the rupture of a so called vulnerable plaque [2]. The susceptibility of a plaque to rupture, its vulnerability, is determined by the morphology and composition of the plaque. The pathological phenotype associated with vulnerable plaques is the thin-cap fibroatheroma (TCFA), characterized by a macrophage infiltrated thin fibrous cap, covering a lipid rich necrotic core [3–5]. The necrotic core contains cholesterol crystals and extracellular droplets of cholesterol esters [6]. When the thin cap ruptures, due to high

#192725 - $15.00 USD Received 21 Jun 2013; revised 29 Jul 2013; accepted 25 Aug 2013; published 5 Sep 2013

mechanical stresses, the lipid rich thrombogenic content of the TCFA can flow freely into the bloodstream and potentially causes an occlusion at the rupture location or downstream from that site. The presence and location of atherosclerotic lipids are therefore important markers of plaque vulnerability.

No established technique can positively quantify and locate the lipid content of atherosclerotic plaques. Intravascular ultrasound (IVUS) produces cross-sectional images of the arterial wall based on the reflected amplitude of ultrasound pulses. Due to minimal contrast between soft tissue constituents, the sensitivity and specificity of IVUS grayscale for plaque composition is limited [7]. IVUS radiofrequency data analysis techniques for tissue characterization, namely VH-IVUS (20 MHz, phased-array transducer, Volcano Therapeutics), and iMap (40 MHz, mechanical-type transducer, Boston Scientific), have been developed as an extension to grayscale imaging [8]. However, the accuracy of VH-IVUS in complex lesions in a porcine model was limited [9, 10]. Significant and systematic variability in plaque composition estimates was found in a study comparing VH-IVUS and iMap in vivo [11]. Intravascular optical coherence tomography (IVOCT) utilizes the delay in backscattered light to form an image of the illuminated tissue. Tissue characterization by IVOCT is currently under development [12]. OCT mainly relies on scattering contrast, which suggests that the chemical specificity is likely to be limited. Near infrared reflection spectroscopy (NIRS) is an intravascular catheter-based technique that utilizes optical absorption to detect lipid-core lesions. It lacks depth resolution, however, and cannot locate the position of the lipid-core relative to the lumen boundary [13]. By combining NIRS with IVUS, morphological imaging is added to lipid detection, but the amount and the location of the lipid relative to the lumen remains unknown [14].

Intravascular photoacoustics is an emerging technique that has the ability to image lipids in atherosclerotic lesions. It utilizes differences in the optical absorption spectra to identify tissue types. A specific tissue type in the arterial wall can be visualized by selecting an excitation wavelength that is strongly absorbed by that particular tissue. The chemical absorption spectrum then represents the molecular composition of the tissue. Well-known applications of spectroscopic PA imaging are detection of exogenous chromophores [15] and quantification of blood oxygenation [16]. The capability of spectroscopic IVPA (sIVPA) to image lipids in human coronary atherosclerotic arteries has been demonstrated ex vivo [17]. More recently, in vivo IVPA imaging of lipids inside the vessel wall of an abdominal rabbit aorta has been shown [18]. Spectral differences between lipid-rich and normal vascular tissue have been outlined by photoacoustic measurements of human aorta samples [19] and pig carotid arteries [20]. In sIVPA, lipid content can be deduced from the photoacoustic spectra or comparison of co-registered IVPA images at different wavelengths.

To be useful in the clinic, as a research tool or to guide percutaneous coronary interventions, however, atherosclerotic lipid content information needs to be readily available without the need for observer-dependent and time-consuming image interpretation. Ideally, only the lipids present within atherosclerotic plaques in the vessel wall are displayed, while the peri-adventitial lipids, which are a component of the normal vessel wall anatomy, remain hidden. That way, in an artery pullback, the cross-sections that contain plaque lipids will be obvious and can be distinguished easily, without clutter by false-positives from normal adipose tissue. For translation to in vivo imaging, where motion artifacts and thus imaging speed play an important role, the number of wavelengths needs to be as small as possible.

In this study, we present a number of methods that provide sIVPA lipid detection in a semi-automated manner. We obtained sIVPA images of a lipid containing vessel phantom using a combined IVPA/IVUS imaging system and catheter. The collected sIVPA data were used to develop the different lipid detection methods. The methods were then fine-tuned and tested on sIVPA data of ex-vivo human coronary arteries, obtained using the same dual modality imaging system.

#192725 - $15.00 USD Received 21 Jun 2013; revised 29 Jul 2013; accepted 25 Aug 2013; published 5 Sep 2013

2. Methods

2.1 Combined intravascular ultrasound and photoacoustic imaging system

The dual modality imaging system for co-registered IVPA/IVUS imaging has been previously developed and described [17]. A tunable laser (OPOTEK Vibrant B/355-II) supplied the excitation light (pulse width 5 ns, repetition rate 10 Hz, pulse energy 1.2 mJ at catheter tip) for photoacoustic imaging. A tapered multimode fiber (Oxford Electronics, Four Marks, UK; input diameter 1 mm; output diameter 360 μm) collected the free space laser light output and delivered it to an in-house designed and built catheter. Two hybrid IVPA/IVUS catheter prototypes were used for this study. They both comprised a 400 μm diameter core optical fiber (Pioneer Optics, Bloomfield, CT) to deliver the light pulses to the vessel wall and an ultrasound transducer to transmit and receive ultrasound waves. The fiber tip was polished under a 34° angle covered by a quartz cap to maintain an air–glass interface deflecting the beam by total reflection. The first prototype, described in detail in earlier work [17], contained a circular lead–zirconium–titanate (PZT) ultrasound transducer with a diameter of 1.0 mm (custom built by TUDelft; design by DuMED [21]). The transducer had a center frequency of 30 MHz, a −6 dB fractional bandwidth of 65% and was mounted distal from the fiber in an assembly with an outer diameter of 1.25 mm. The second prototype held a 0.4 by 0.4 mm lead magnesium niobate-lead titanate (PMN-PT) single crystal ultrasound transducer (designed and custom built by the University of Southern California, Department of Biomedical Engineering [22]) with a center frequency of 44.5 MHz and a −6 dB fractional bandwidth of 45%. Fiber and transducer were mounted in an assembly with an outer diameter of 1 mm. In both prototypes, the fiber tip and transducer center were separated by approximately 1 mm and the optical and acoustical beam overlapped between 0.5 and 4.5 mm from the transducer, with an angle of 22°.

An arbitrary waveform generator (Tabor Electronics WW2571A) transmitted a Gaussian-modulated cosine wave for pulse echo imaging, which was transmitted to the probe through a custom-built expander and limiter. The catheter was rotated using a motorized rotary stage (Steinmeyer GmbH & Co. KG). The received US and PA signals were band pass filtered (13–60 MHz 5th order Butterworth, custom built), amplified by a 43 dB amplifier (Miteq AU1263) and digitized at a sample frequency of 350 MS s^{-1} by a 12-bit data acquisition card (Acqiris DP310).

2.2 Phantom design

We designed and constructed a vessel mimicking poly-vinyl-alcohol (PVA, 10% wt. PVA crystals in demineralized water, 2 freeze/thaw cycles) phantom with a 3 mm diameter lumen and four 1.5 mm round by 5 mm deep cylindrical cavities at 500 μm from the lumen. One cavity was filled with peri-adventitial tissue that we obtained from one of the human coronary artery specimens, see description below. In peri-adventitial tissue, lipids are stored as a mixture of fatty acids [23]. The other three cavities were filled with cholesterol, cholesterol oleate and cholesterol linoleate (Sigma Aldrich Co., C8667, C9253 and C0289, resp.). These three compounds are the most abundant lipids in atherosclerotic lesions [24, 25], and are assumed to be representative of plaque lipids.

Reference absorption spectra of pure cholesterol, cholesterol linoleate, cholesterol oleate, and of peri-adventitial tissue, were acquired by recording the wavelength-dependent PA signal. The respective lipids were held in a container made of TPX (TPX® Polymethylpentene) in a water bath in such a way that the there was a clear optical and acoustic path between the probe and the target. The data were averaged and processed to obtain spectra that were reproducible in time and depth, see Fig. 1(a).

#192725 - $15.00 USD Received 21 Jun 2013; revised 29 Jul 2013; accepted 25 Aug 2013; published 5 Sep 2013

2.3 Coronary artery acquisition and handling

We collected human coronary arteries at autopsy from the Department of Pathology of the Erasmus Medical Center (MC). We obtained consent from the relatives and our research protocol was approved by the Medical Ethics Committee of the Erasmus MC (MEC-2007-081). The coronary arteries were measured freshly within 24h post mortem or frozen within 4h at −80° to be thawed and measured at a later date.

2.4 Combined photoacoustic and ultrasound imaging

We acquired combined photoacoustic and ultrasound images of the lipid containing vessel phantom and the human coronary arteries ex vivo. The vessel phantom was placed in a water bath, after which we inserted our combined IVPA/IVUS catheter in the lumen and recorded co-registered IVPA/IVUS cross-sectional data. The coronary arteries were placed in a holder and mounted on two cannulas in a water tank containing saline solution at room temperature. The holder was made of TPX with thin (200 μm) metal wires glued at every 1.5 mm perpendicular to the longitudinal axis to mark imaging locations. We then performed an IVUS pullback of the arteries using a commercial IVUS system (Boston Scientific iLab, Atlantis SR Pro catheters) to find sites of interest. Using our combined IVPA/IVUS catheter, the selected wires were found and at these locations co-registered IVPA and IVUS cross-sectional scans were made.

To create the ultrasound images, we transmitted a 10 V peak to peak Gaussian-modulated cosine wave with a center frequency of 30 MHz and a 100% bandwidth for the first prototype catheter and a center frequency of 44.5 MHz and a 50% bandwidth for the second prototype catheter. Transmission bandwidths are specified at a −6dB level relative to the peak. With the exception of the phantom and first artery, the results of which are shown in Fig. 2 and Fig. 3, respectively, all arteries were measured using the second prototype catheter (44.5 MHz center frequency).

We acquired IVPA images at several excitation wavelengths around 1200 nm. In this wavelength range, the second overtone of C-H bond vibrations within the different structural groups of the lipid molecules produce several overlapping peaks in the lipid absorption spectra. By staying within a relatively narrow wavelength range, we ensured that variations in the laser pulse energy and tissue scattering properties are negligible.

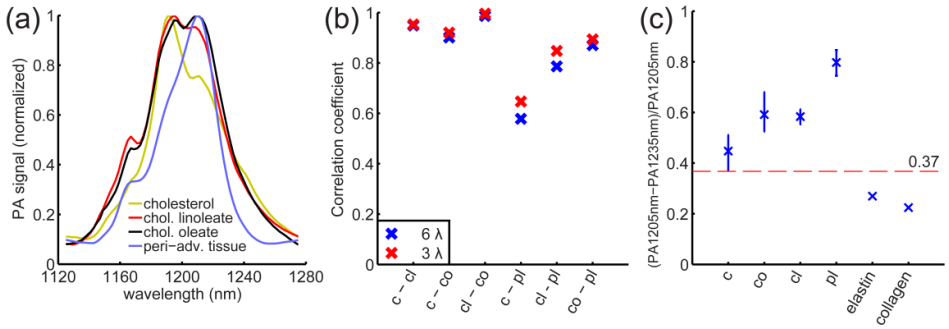

Fig. 1. (a) Normalized reference PA spectra of cholesterol, cholesterol linoleate, cholesterol oleate, and peri-adventitial tissue, measured on the pure compounds. (b) Correlation coefficients between the 6 and 3-wavelength PA spectra of the different lipid types. (c) 5th to 95th percentile of the relative difference of 1205 nm and 1235 nm PA signal strength of cholesterol, cholesterol oleate, cholesterol linoleate and peri-adventitial lipids (672, 864, 512 and 372 spectra, respectively). The values for elastin and collagen are taken from literature [23]. c = cholesterol; cl = cholesterol linoleate; co = cholesterol oleate; pl = peri-adventitial lipids.

Two-dimensional spatially co-registered spectroscopic IVPA and IVUS images were obtained by rotating the catheter in 1° steps and repeating the photoacoustic and ultrasound

#192725 - $15.00 USD Received 21 Jun 2013; revised 29 Jul 2013; accepted 25 Aug 2013; published 5 Sep 2013

acquisitions at every step. IVUS images were obtained by averaging the echoes from 10 transmissions per line; IVPA was not averaged (one laser pulse per image line). At every angle, the laser was tuned through the spectral range of interest to ensure co-registration of the IVPA data at all wavelengths. Digitized IVPA and IVUS data were band pass filtered between 10 and 40 MHz and 10 and 70 MHz for the first and second catheter prototype, respectively (100th order zero-phase forward and reverse finite impulse response (FIR) filter). Filtered data were upsampled, corrected for jitter and downsampled to the original sampling frequency. Data that was affected by (environmental) noise benefited from additional median filtering in the angular direction, this concerned arteries 2 and 4 (kernel width 3° and 5°, respectively).

IVPA data can be affected by an artifact caused by the absorption of laser pulses in the ultrasound transducer and catheter tip. It shows up in the images as bright rings, concealing the photoacoustic signals produced by the arterial tissue close to the probe. An adaptive filter was designed and applied to the IVPA data to remove this artifact. The IVUS data contained a similar circular artifact, caused by the 'ringing' of the transducer as a result of the transmission of ultrasound pulses, that we removed by subtracting the mean in the angular direction of the affected part of the data. Both the IVPA and IVUS data were then Tukey windowed and envelope filtered. The spectroscopic IVPA data was corrected for variations in the light energy between individual pulses and between the different wavelengths, using the amplitude in the ring artifact mentioned above. The data were subsequently scan-converted to Cartesian coordinates and log compressed. We used the 'hot' and 'gray' colormaps in Matlab (R2007b) to display the IVPA and IVUS images, respectively. Combined IVPA/IVUS images were created by overlaying the IVPA data on the IVUS images using a nonlinear red-yellow-white color scale and a linear transparency scale. All data processing was done using Matlab (R2007b).

After imaging, the arteries were cut at the two wires adjacent to the imaging planes to obtain 3 mm thick artery segments with the imaged cross-section in the middle. The segments were embedded in optimal cutting temperature (OCT) compound (Tissue-Tek®, Sakura Finetek Europe B.V.), frozen in liquid nitrogen cooled isopentane vapor, and stored at −80 °C until serial sectioning for staining. Oil Red O (ORO) staining was performed to identify lipids (stained red). A Hematoxylin-Eosin (H&E) stain was used as an overview stain. To demonstrate the morphology and fibrous structure of the vessel cross-sections, a Resorcin-Fuchsin (RF) stain was used.

2.5 Lipid detection methods

Per imaging location, the spatially co-registered sIVPA data were used to obtain the lipid distribution within the vessel wall. We imaged a cross-section of the vessel phantom and the first artery at six equally spaced wavelengths between 1185 and 1235 nm. Acquistion of a full image at six wavelengths is a time-consuming procedure, mainly because the laser takes time to tune. To limit tissue degradation, we performed 6-wavelength imaging on one vessel only. The data were first processed as described above, up to scan-conversion. Then, for each pixel in the resulting data set, the correlation coefficient $R_{n=6}$ (n is the number of wavelengths) of the 6-wavelength PA spectrum with two different reference spectra was computed. We used the PA spectra of cholesterol and peri-advential tissue as reference spectra for plaque and peri-adventitial lipids, respectively. The correlation coefficients between the various spectra [Fig. 1(b)] show that the cholesterol spectrum has the lowest correlation with the peri-adventitial spectrum and therefore is the most suitable to distinguish plaque from other lipids.

The 6-wavelength correlation coefficients $R_{x,6}$ (x is lipid type; "c" for cholesterol or "pl" for peri-adventitial lipids) were median filtered over 4° in the angular direction and 8 samples in the radial direction. The threshold values $R_{\mathrm{th},x,6}$ for the correlation coefficients were chosen empirically as the lowest values for which plaque lipids could be separated from peri-adventitial lipids. This exercise was performed in the phantom and in the artery specimens,

#192725 - $15.00 USD Received 21 Jun 2013; revised 29 Jul 2013; accepted 25 Aug 2013; published 5 Sep 2013

discriminating lipid type based on location inside or outside the vessel wall. The lipid matching regions – those with a correlation coefficient equal to or higher than the threshold $R_{th,x,6}$ – were colored red and overlaid on the corresponding IVUS image to create a lipid map.

We investigated the potential for identification and differentiation of the lipids using three and two wavelengths only. Several combinations of three wavelengths within the 1185–1235 nm range were tested on the 6-wavelength data sets of the phantom and first artery. A three wavelength correlation will necessarily suffer more from accidental high correlation of the noise with the reference spectrum than a six wavelength correlation and therefore can be improved by applying a mask that cuts off the data at the noise level. We determined the noise level at 1205 nm by sampling the PA signal inside the lumen (identified in the IVUS image). All PA signal below that level was masked out. In these masked data, lipids were then detected in a manner similar to the 6-wavelength data sets, and a new pair of correlation coefficients $R_{th,x,3}$, was chosen for both the phantom and artery measurement.

Two-wavelength lipid detection was implemented using sIVPA data obtained at 1205 and 1235 nm. At 1205 nm, lipid absorption is high, while at 1235 nm, the lipid absorption is reduced by 40 to 85%. Lipid maps were computed using the following algorithm: we determine the noise level at 1205 nm by sampling the PA signal inside the lumen (which can be identified in the IVUS image). All PA signal below that level is masked out. We compute the relative difference $\delta = [I_{1205} - I_{1235}]/I_{1205}$, where I_λ is the PA signal amplitude at wavelength λ. δ is median filtered (4° angular by 8 samples radial). Lipids are identified by $\delta > \delta_{th} = 0.37$, where δ_{th} is a threshold value determined from the analysis of the absorption spectra of pure lipids, see Fig. 1(c). We applied this method to the sIVPA data at 1205 and 1235 nm of the phantom and at several cross-sections of the human coronary arteries.

3. Results

3.1 Phantom

We performed IVPA/IVUS on a lipid-containing vessel phantom at 6 evenly spaced wavelengths from 1185 to 1235 nm. The co-registered combined IVPA/IVUS images at 1205 and 1235 nm are shown in Figs. 2(a) and 2(b), respectively. All four lipid containing cavities exhibit an increased PA signal at 1205 nm compared to the PA signal at 1235 nm. The lipid map resulting from the 6-wavelength correlation with the cholesterol reference spectrum, Fig. 2(d), detects the cholesterol and cholesterol esters, representative of plaque lipids, while the peri-adventitial tissue remains concealed. The correlation with the peri-adventitial reference spectrum, Fig. 2(e), results in detection of the peri-adventitial tissue, while suppressing the other lipids. Figure 2(f) illustrates the resemblance of the average IVPA spectra in the lesion area indicated by the green sector in Fig. 2(d), and the peri-adventitial area (blue sector in Fig. 2(e)), with their respective reference spectra. The atherosclerotic plaque and peri-adventitial lipid maps created using the 3 wavelength correlation with the associated reference spectra, overlaid on the IVUS image, are shown in Figs. 2(g) and 2(h), respectively. The results shown here are obtained using 1185, 1205 and 1235 nm, which was the combination of wavelengths that resulted in the most specific separation between plaque and peri-adventitial lipids. The result of the 2-wavelength relative difference method using 1205 and 1235 nm is shown in Fig. 2(i). The method succeeds to display all the lipid regions well, but does not distinguish between atherosclerotic and peri-adventitial lipids.

#192725 - $15.00 USD Received 21 Jun 2013; revised 29 Jul 2013; accepted 25 Aug 2013; published 5 Sep 2013

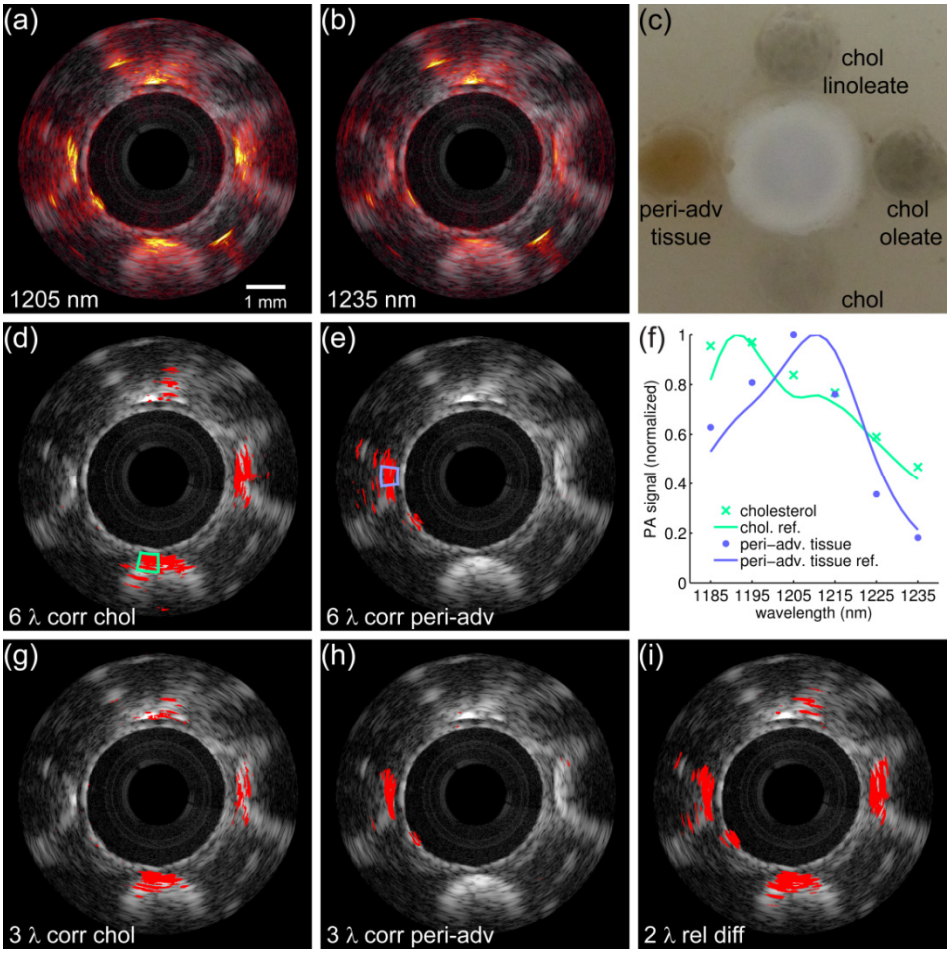

Fig. 2. Lipid-detection in a lipid-containing vessel phantom. (a) 1205 nm and (b) 1235 nm combined IVPA/IVUS images (IVPA 50 dB, IVUS 65 dB) of PVA phantom filled with cholesterol (bottom), cholesterol oleate (right), cholesterol linoleate (top) and peri-adventitial tissue (left). (c) Photograph of the phantom (top-view). Lipid map based on 6-wavelength correlation with the cholesterol (d) and peri-adventitial reference spectrum (e). (f) Average IVPA signal spectra in the cholesterol and peri-adventitial tissue areas indicated in (d) and (e), respectively, are highly correlated with their respective reference spectra. Lipid map based on 3-wavelength correlation with the cholesterol (g) and peri-adventitial reference spectrum (h). (i) Lipid map based on 2-wavelength relative difference. All lipid maps are shown overlaid on the corresponding IVUS image.

Table 1 lists the threshold correlation values $R_{\text{th},x,6}$ and $R_{\text{th},x,3}$ for 6 and 3 wavelengths respectively, which were used to create the lipid maps in Figs. 2(d)–2(e) and 2(g) –2(h). The 3-wavelength correlation method distinguishes equally well between the two lipid types as the 6-wavelength correlation. A slight decrease in the amount of lipids detected can be seen, however, which is caused by the addition of the noise masking step.

3.2 Arteries

IVPA/IVUS was performed on a human coronary artery specimen exhibiting early stage atherosclerosis (left anterior descending artery, female aged 41, imaged < 24 h post mortem). Figures 3(a) and 3(b) show the co-registered combined IVPA/IVUS images at 1205 nm (high lipid absorption) and 1235 nm (low lipid absorption), respectively. In the IVUS image, the luminal border and the external elastic lamina are clearly visible. The images show two

#192725 - $15.00 USD Received 21 Jun 2013; revised 29 Jul 2013; accepted 25 Aug 2013; published 5 Sep 2013

thickened intimal regions that exhibit a brighter signal in the 1205 nm IVPA image than in the 1235 nm IVPA image. A brighter signal is also observed in the 1205 nm IVPA image in the peri-adventitial regions all around the vessel. The corresponding lipid stain, shown in Fig. 3(c), confirms the presence of lipids in the regions with enhanced 1205 nm IVPA signal. The three different lipid detection methods were applied to the co-registered IVPA data. The obtained optimal threshold values $R_{th,x,n}$, listed in Table 1, differ slightly from those found with the phantom data but show a similar trend. The findings are comparable to the lipid detection results in the phantom: Fig. 3(d) clearly depicts the lipids in the fatty streak at the bottom right while suppressing successfully the peri-adventitial lipids. However, it fails to distinctly show the lipids present in the smaller fatty streak at the top of the vessel. In contrast, Fig. 3(e) depicts the peri-adventitial lipids while suppressing the lipids present within the thickened intima. The plaque and peri-adventitial lipid maps created using the 3 wavelength (1185, 1205 and 1235 nm) correlation with the associated reference spectra, overlaid on the IVUS image, are shown in Figs. 3(g) and 3(h), respectively. The 3-wavelength correlation with cholesterol seems to be working equally well as the 6-wavelength correlation, whereas the 3-wavelength peri-adventitial lipid correlation degrades slightly. The result of the 2-wavelength relative difference method using 1205 and 1235 nm is shown in Fig. 2(i). As in the phantom case, the method succeeds to display all the lipid regions well, but does not distinguish between atherosclerotic and peri-adventitial lipids. Note that all lipid detection methods effectively suppress the strong PA signal from the wire that can be seen at the top of the IVPA images in Fig. 2(a) and (b).

Subsequently, we acquired co-registered IVPA/IVUS images at 1205 and 1235 nm of several human coronary arteries exhibiting varying degrees of atherosclerosis. The lipid maps resulting from the 2-wavelength lipid detection method, overlaid on the IVUS images, are shown in Figs. 4, 5, and 6 with collocated histology, always showing the ORO stain. Figure 4 demonstrates the lipid detection method on a healthy coronary artery (left anterior descending artery, male aged 65, imaged after frozen storage). Lipids are found in the peri-adventitial tissue only; this is confirmed by the lipid histology stain. The peri-adventitial fat is a very fragile structure, and as a result some of it has fallen off in tissue handling after imaging.

Table 1. Threshold Values $R_{th,x,n}$ and δ_{th}

Method	Threshold variable	Phantom	Artery
6 λ	$R_{th,c,6}$	0.88	0.93
	$R_{th,pl,6}$	0.85	0.85
3 λ	$R_{th,c,3}$	0.96	0.98
	$R_{th,pl,3}$	0.96	0.95
2 λ	δ_{th}	0.37	

#192725 - $15.00 USD Received 21 Jun 2013; revised 29 Jul 2013; accepted 25 Aug 2013; published 5 Sep 2013

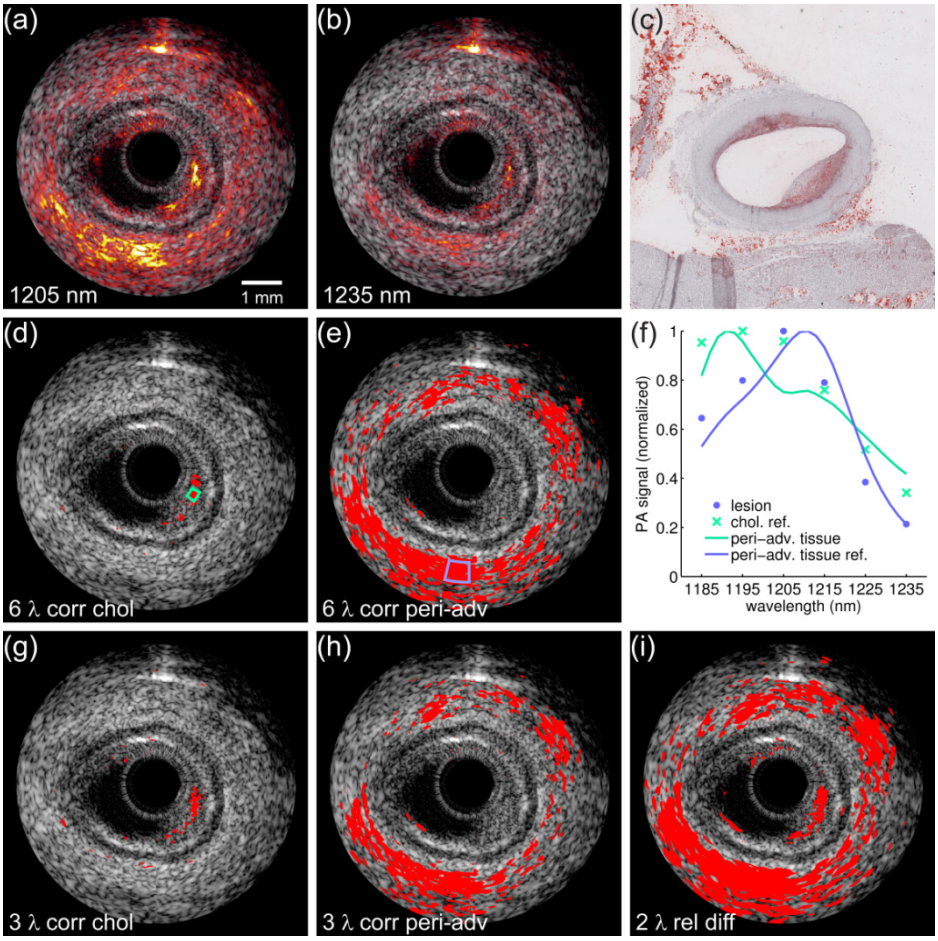

Fig. 3. Lipid detection in an early stage atherosclerotic human coronary artery. (a) 1205 nm and (b) 1235 nm combined IVPA/IVUS images (IVPA 35 dB, IVUS 40 dB). (c) Lipid histology stain (ORO); lipids are stained red. Lipid map based on 6-wavelength correlation with the cholesterol (d) and peri-adventitial reference spectrum (e). (f) Average IVPA signal strength in the lesion and peri-adventitial areas indicated in (d) and (e), respectively, shows high correlation with the respective reference spectra. Lipid map based on 3-wavelength correlation with the cholesterol (g) and peri-adventitial reference spectrum (h). (i) Lipid map based on 2-wavelength relative difference. All lipid maps are shown overlaid on the corresponding IVUS image.

Two sites in an atherosclerotic human coronary specimen (left anterior descending artery, male aged 80, imaged after frozen storage) are shown in Fig. 5. The IVUS image in Fig. 5(a) shows a narrowed lumen with two plaques at the top right and the bottom of the vessel wall. The shadowing deeper in the plaque area at the bottom of the image indicates the presence of a calcification. These findings are confirmed by the ORO lipid stain, which is depicted in Fig. 5(b). The lipid map, overlaid on the IVUS image, shows lipids in both the bottom and top plaque regions, accurately collocated with the atherosclerotic lipids visible in the lipid histology stain. The peri-adventitial lipids are only visible in the lipid map on the top left and bottom right, where the light and ultrasound waves penetrate deep enough to reach the tissue surrounding the vessel. At the next imaging location, excellent agreement between the lipid map overlaid on the IVUS image and the lipid histology stain is observed. The lipid stain

#192725 - $15.00 USD Received 21 Jun 2013; revised 29 Jul 2013; accepted 25 Aug 2013; published 5 Sep 2013

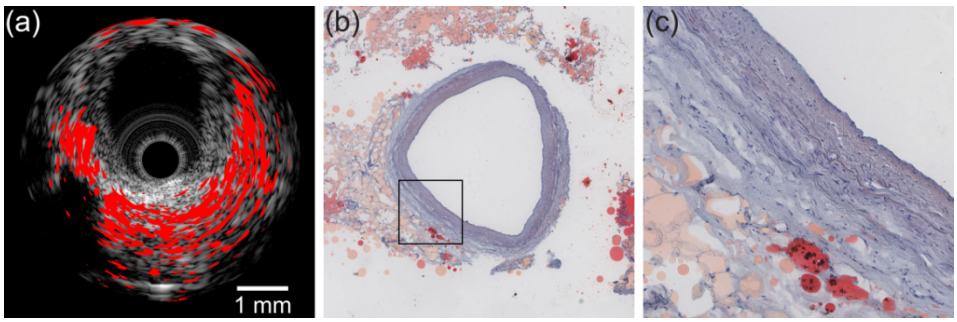

Fig. 4. Lipid detection in a healthy human coronary artery. (a) Lipid map based on relative difference between PA signal at 1205 and 1235 nm, overlaid on IVUS image (40 dB). (b) Lipid histology stain (ORO). (c) 5 x magnification of a part of the healthy vessel wall and peri-adventitial lipids (area outlined in black in (b)). Both in the lipid map and the lipid stain, lipids are found in the peri-adventitial region only.

reveals an eccentric plaque, with lipids located at specific locations in the lesion, see Figs. 5(e)–5(i). The lipid map assesses these lipid rich locations accurately. The peri-adventitial lipids appear in all directions except behind the plaque, where the vessel wall is thickened considerably.

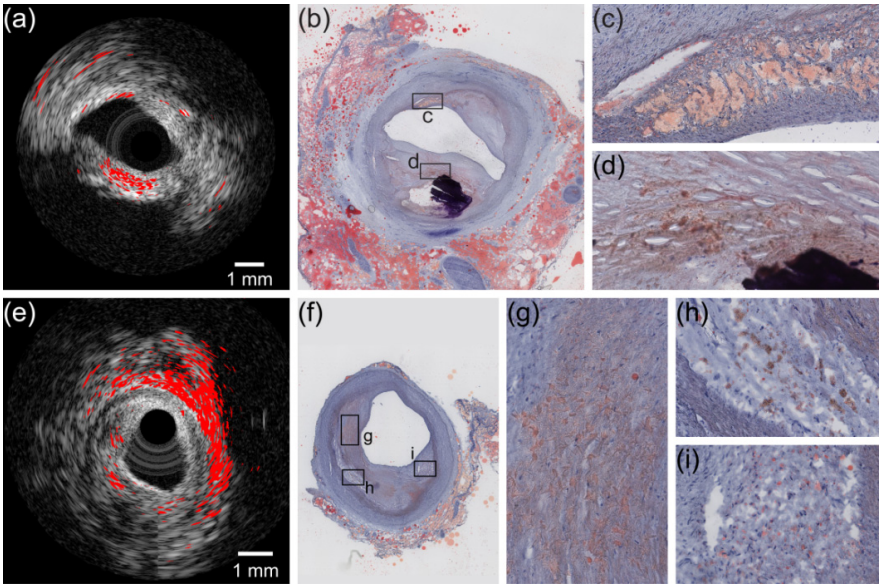

Fig. 5. Lipid detection in a diseased coronary artery. (a) Lipid map at first imaging location, based on relative difference between PA signal at 1205 and 1235 nm after masking the noise, overlaid on IVUS image (45 dB). (b) Corresponding lipid histology stain (ORO). Lipids are found in the top and bottom plaque areas, as well as in the peri-adventitial region, in correspondence with the lipid stain. 10x magnifications of area c and d are shown in (c) and (d), respectively. (e) Lipid map, created using the same 2-wavelength method, overlaid on 45 dB IVUS image, and (f) lipid histology stain at second imaging location. The lipid map displays all locations with extracellular lipid droplets and cholesterol (areas g, h and i, shown 10x magnified in (g), (h) and (i), respectively) accurately. Peri-adventitial lipids that are located beyond the lesion are obscured.

Figure 6 shows the results of the combined IVPA/IVUS measurement of an eccentric plaque with diffuse intracellular lipid according to histology (left anterior descending artery, female aged 51, imaged fresh). The lipid-rich eccentric plaque, as imaged by IVPA, has a mottled appearance due to the lipids that are scattered throughout most of the lesion. The lipid

#192725 - $15.00 USD Received 21 Jun 2013; revised 29 Jul 2013; accepted 25 Aug 2013; published 5 Sep 2013

map closely mimics the appearance of the plaque by showing small lipid specks distributed throughout the plaque region. Small lipid deposits in the vessel wall opposite the lesion and the larger lipid deposits of the peri-adventitial tissue show up as well.

4. Discussion and conclusions

This study demonstrates that spectroscopic intravascular photoacoustic imaging can automatically detect atherosclerotic and peri-adventitial lipids, as well as distinguish between them, with a small number of excitation wavelengths. We have developed and tested a number of, progressively simpler, methods using the co-registered sIVPA/IVUS data we acquired in a lipid containing vessel phantom and several human coronary arteries ex vivo. Correlation with a cholesterol PA spectrum, as reference for atherosclerotic lipids, and with a peri-adventitial reference spectrum, using 6 equally spaced wavelengths from 1185 to 1235 nm, distinguishes very well between atherosclerotic lipids and peri-adventitial lipids. Correlation using just 3 well-chosen wavelengths within this wavelength range, namely 1185, 1205 and 1235 nm, still achieves a satisfactory distinction between these two lipid types. Utilizing the relative difference between the PA signal at 1205 and 1235 nm, we successfully detected both the atherosclerotic and peri-adventitial lipids in several human coronary arteries. Separate depiction of the two lipid types was not achieved, even though PA data of the pure compounds [Fig. 1(c)] suggest this as a possibility. In actual tissue, however, variability in optical properties and a lower signal-to-noise level preclude separation of lipid types.

Evaluation of two-wavelength sIVPA in human coronary arteries ex vivo shows the appearance of different manifestations of disease, compared to histology: Fig. 4 shows a healthy artery, which by IVPA is characterized by an absence of lipid signal in the intima and media. Figures 5 and 6 compare large lipid deposits [Figs. 5(c) and 5(d)] with small [Figs. 5(g)–5(i)] and larger [Fig. 6] extracellular lipid droplets. The lipid distribution by IVPA closely follows the histological appearance.

Other methods have been reported for separating lipids from other tissue types [26], relying on the acquisition of more wavelengths. This richer spectral sampling may increase robustness against measurement noise, permits automated spectral unmixing [27], and possibly enhances chemical detail. A drawback is, however, that additional wavelengths lower the imaging speed proportionally, lengthening the acquisition time and increasing the

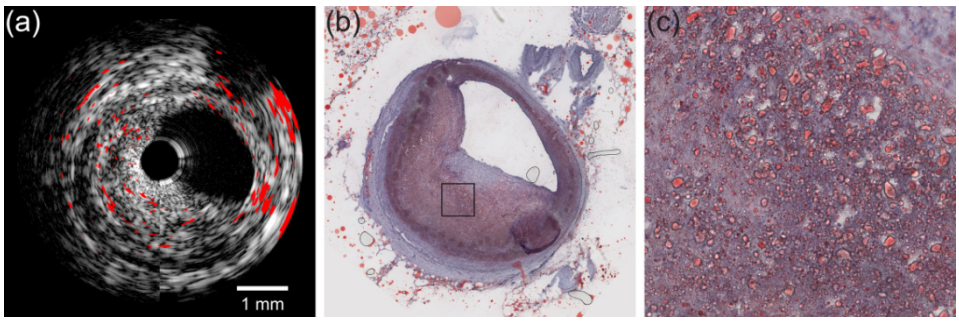

Fig. 6. Lipid detection in a coronary artery with an eccentric atherosclerotic lesion with lipids distributed throughout the plaque. (a) Lipid map based on relative difference between PA signal at 1205 and 1235 nm after masking the noise, overlaid on IVUS image (30 dB). (b) Lipid histology stain (ORO). (c) 10 x magnification of part of the plaque (area outlined in black in (b)). The distributed plaque lipids are displayed in the lipid map as small red marks throughout the lipid containing area.

susceptibility to motion artifacts. For in vivo imaging, the number of wavelengths should be kept as small as possible. The difference in our approach compared to other techniques in the literature does complicate a direct performance comparison.

#192725 - $15.00 USD Received 21 Jun 2013; revised 29 Jul 2013; accepted 25 Aug 2013; published 5 Sep 2013

Catheter-based coronary imaging is usually performed by pulling back the catheter inside the artery under investigation, as it rotates. In this way, a large, volumetric data set is accumulated, which is reviewed during or after acquisition. A technology that automatically identifies lipid-rich plaques in the vessel greatly simplifies the review and interpretation process, and development of this functionality is one of the main drivers of this study. In principle, segmentation of the peri-adventitia based on the IVUS image is possible. In practice, however, automated IVUS image analysis has proven to be a very difficult problem, which is why we propose to exploit the chemical differences that exist between plaque lipids and others to generate image contrast.

Incomplete depiction of the topmost fatty streak in the correlation lipid maps of the human coronary artery specimen imaged using six wavelengths [Figs. 3(d) and 3(g)], was caused by filtering the data for artifact reduction, as discussed in section 2.4. The filter is nonlinear and this affects the spectral correlation that we compute. The 2-wavelength analysis [Fig. 2(i)] appears to be more robust, retaining the feature partially. The catheter design will be adapted to considerably reduce this artifact in future experiments. In the peri-adventitial [Figs. 3(e) and 3(h)], as well as the 2-wavelength lipid map [Fig. 3(i)], of the same cross-section, a thin lipid-positive layer can be seen at the bottom left of the luminal border that is unmatched by histology. A piece of adipose tissue may have been moved into the lumen in preparation for the experiment, and subsequently dislodged by tissue handling.

This qualitative study demonstrates the viability of detecting arterial lipid with a limited number of wavelengths. It will be compounded in the future with a larger quantitative study to establish the optimal experimental and analysis procedures. Such a study should also include a statistical analysis to quantify the sensitivity and specificity of IVPA for lipid-rich plaque detection. Our findings seem to indicate a high sensitivity for extracellular lipid droplets, as illustrated in Fig. 6, while intracellular lipids remain mostly undetected. The selection of wavelengths may be further optimized to improve sensitivity. Alternatively, sensitivity might be increased by imaging in the 1700 nm wavelength range, where lipid absorption is much higher [18, 26]. Tradeoffs exist in the form of a high water absorption, which may present a challenge in this wavelength range, and the chemical specificity of the absorption spectra of the different lipids, which remains to be explored. Further automation of the analysis could be achieved by automatic contour detection in IVUS to determine the luminal noise level. The dynamic range in the images was adjusted to accommodate the dynamic range of the acquired data.

In summary, we presented an analysis of sIVPA data to detect atherosclerotic lesion lipid content in a semi-automated fashion and with high resolution. The methods were demonstrated on human coronary arteries ex vivo and have the potential to be used in an in vivo setting. Automatic depth-resolved lipid detection of human coronary atherosclerosis may find an important role in the clinical detection and treatment, as well as the expansion of our understanding, of coronary artery disease.

Acknowledgments

We thank G. Springeling for catheter assembly and setup design. B. Blokker, E. Krpelanova and N. van der Graaf for collection of the arteries, and R. van Haeren and K. Kuijt-van Gaalen for assistance in histopathology. We thank G. van Dijk (Delft University of Technology) and X. Li (University of Southern California) for providing ultrasound transducers. We also thank D. Maresca and P. Kruizinga for helpful discussion on the experimental design and results. This work was funded by the Dutch Technology Foundation (STW) through the 2007 Simon Stevin Meester grant (STW 10040) to A.F.W. van der Steen.